

Intermediate-Mass Black Hole Formation from Hierarchical Mergers in Galactic Nuclei

AMANDA NEWTON  ^{1,2} SANAEA C. ROSE  ² FULYA KIROĞLU  ² BAO MINH HOANG  ^{3,4} AND FREDERIC A. RASIO ²

¹ Loyola University Chicago, 6460 N Kenmore Ave, Chicago, IL 60660, USA

² Center for Interdisciplinary Exploration and Research in Astrophysics (CIERA) and Department of Physics and Astronomy, Northwestern University, 2145 Sheridan Road, Evanston, IL 60201, USA

³ Department of Physics and Astronomy, University of California, Los Angeles, Los Angeles, CA 90095, USA

⁴ Kall Morris Inc, 130 W Washington St, Marquette, MI 49855, USA

ABSTRACT

Dense stellar environments like nuclear star clusters (NSCs) can dynamically assemble gravitational wave (GW) sources. We consider a population of single stellar mass black holes (BHs) in the inner 0.1 pc of a NSC surrounding a $4 \times 10^6 M_{\odot}$ supermassive black hole (SMBH). Using a semianalytic model, we account for direct collisions between BHs and stars and GW capture between BHs. We explore the effect of the initial BH mass and spin distributions on their final properties and the production of GW sources. Specifically, we consider upper and lower limits for the BH initial mass distribution, and we account for the possibility that a subset of our initial population are the merger products of primordial BH binaries. We find that $\sim 500 M_{\odot}$ intermediate mass black holes (IMBHs) can form for our upper limit mass distribution, while our lower limit mass distribution forms none. Most IMBHs $\gtrsim 200 M_{\odot}$ eventually sink towards the center of the cluster and merge with the SMBH. We also find that BH-star collisions create a more uniform spin distribution. Our results have implications for LIGO-Virgo-KAGRA sources. We find that the overall merger rate depends primarily on the upper limits of the initial BH mass distribution, ranging from $\sim 10^{-10}$ to $\sim 10^{-9} \text{ yr}^{-1}$ per galaxy. However, primordial binaries increase the number of second and higher generation mergers by an order of magnitude.

Keywords: Galactic center (565), Gravitational wave sources (677), Intermediate mass black holes (816), Stellar mass black holes (1611), Stellar dynamics (1596)

1. INTRODUCTION

The detection of gravitational waves (GWs) from merging compact objects has fundamentally changed the way we sense the Universe. Detections by the LIGO-Virgo-KAGRA Collaboration have provided new insights into the demographics of black holes (BHs) (e.g., Fishbach et al. 2020), even in some cases challenging our previous understanding of these populations. Event GW190521, for example, produced an intermediate-mass BH (IMBH) (Abbott et al. 2020), as did the recent event GW231123, the most massive merger detected to date (Abac et al. 2025). Furthermore, the progenitor BHs in these events lie in the pair-instability mass gap, above the maximum BH mass predicted by many stellar evolution models (e.g., Heger et al. 2003; Woosley 2017;

Spera & Mapelli 2017; Limongi & Chieffi 2018; Sakstein et al. 2020; Belczynski et al. 2020; Renzo et al. 2020; Vink et al. 2021), while several GW events, including GW231123, have components with non-zero spins, indicating dynamical formation (e.g. Abac et al. 2025; Tong et al. 2025).

Dense stellar clusters have long been recognized as important contributors to GW sources (e.g., Quinlan & Shapiro 1987; Rodriguez et al. 2018; Rodriguez et al. 2019). The detected highly spinning BHs, several of which lie in the pair-instability mass gap, may be the product of sequential BH mergers from close dynamical interactions in dense clusters (e.g., Antonini & Rasio 2016; Fishbach et al. 2017; Kimball et al. 2021; Fragione et al. 2020). However, GW recoil kicks can pose a problem for globular clusters with typical escape speeds of 50 km/s; the velocity kick from asymmetric GW emission can eject merger products from the cluster (e.g., Schmittman & Buonanno 2007; Centrella et al. 2010;

O’Leary et al. 2006; Baibhav et al. 2020). Recently, Mai et al. (2025) showed that the most massive globular clusters can retain merger products and go on to form second generation and higher mergers similar to those observed by LIGO-Virgo-KAGRA. Similarly, nuclear star clusters (NSCs) have deep potential wells and can retain merger products, as has been shown for NSCs without supermassive black holes (SMBHs) (e.g., Miller & Lauburg 2009; Antonini & Rasio 2016; Fragione et al. 2021). In one relevant dynamical process, single BHs which approach each other closely may radiate enough energy via GWs to become a bound system. O’Leary et al. (2009) find GW capture rates of $\sim 10^{-10}$ to $\sim 10^{-9}$ yr $^{-1}$ per galaxy for a population of single BHs in a NSC with a SMBH, though they did not detail the specific merger generation or mass and spin properties of those events. More recently, Liu & Lai (2025) considered a broad range of dynamical interactions, focusing on binary-single interactions that form second generation/second generation (2G/2G) mergers in NSCs.

The presence of a SMBH can increase the potential for these environments to generate GW sources. A SMBH can induce binary systems in its vicinity to merge by exciting their orbital eccentricities, in a process known as the Eccentric Kozai-Lidov (EKL) Mechanism (e.g., Kozai 1962; Lidov 1962; Naoz et al. 2013a,b; Naoz 2016). This process can lead to the merger of BH binaries which, if left on their initial orbit, would otherwise not have merged within a Hubble time (e.g., Antonini & Perets 2012; Antognini et al. 2014; Hoang et al. 2018; Fragione et al. 2018; Su 2025; Stegmann et al. 2025; Grishin et al. 2025). In addition to BH-BH interactions, dense stellar environments facilitate direct collisions between BHs and stars (e.g., Bailey & Davies 1999; Davies et al. 2011; Rose et al. 2022; Kiroğlu et al. 2025a). Rose et al. (2022) show that frequent collisions between BHs and stars in nuclear star clusters can create more massive BHs, some $> 100 M_{\odot}$ (for a similar process in globular clusters, see Rizzuto et al. 2022). In addition to shaping the BH mass demographics, the subsequent accretion of material from the star can have detectable implications for the BH spins (Lopez et al. 2019; Kiroğlu et al. 2025b,c).

Future and ongoing GW observational campaigns motivate our study of the rates and properties of merger events from NSCs, as well as the processes shaping the broader BH population in these environments. We expand the model in Rose et al. (2022), which accounts for BH-star collisions and two-body relaxation, to include GW capture between single BHs. We vary the initial BH mass and spin distributions and consider the possibility that a fraction of the BHs in our initial pop-

ulation come from already-merged primordial binaries, based on the results of Hoang et al. (2018). Our goal is to determine how the initial conditions affect the dynamical fate of the BHs, including the production of GW sources, and map onto the final property distributions. We also assess the feasibility of forming IMBHs (BHs with mass $> 100 M_{\odot}$) in NSCs. Our paper is organized as follows:

In Section 2, we give an overview of our semianalytic model for the evolution of BHs in a NSC with an SMBH. In particular, Section 3 describes our initial conditions and Section 4 describes the physical processes we consider in a cluster. We present and discuss results in Section 5, including signatures of dynamical processes in the mass and spin distributions of the BHs in Sections 5.1 and 5.3, IMBH formation in Section 5.4, and implications for GW sources in Section 5.5.

2. OVERVIEW OF SEMIANALYTIC MODEL

We use a semianalytic model first developed by Rose et al. (2022) to study the dynamical evolution of a cluster of BHs in a NSC like the Milky Way’s, with a central $4 \times 10^6 M_{\odot}$ SMBH. For the purposes of this study, we assume the NSC is composed of $1 M_{\odot}$ stars and BHs with initial masses described in Section 3. We follow a sample of 1000 BHs embedded in a NSC over an integration time of 10 billion years, tracking their properties at each timestep. We draw their initial masses, spins, and orbital properties statistically as described in Section 3 so that they are representative of the overall BH population.

While we only follow a sample of 1000 BHs, our model accounts for the presence and effects of the surrounding star cluster using a statistical approach and timescale arguments. The surrounding cluster can be described by two key properties, the density and velocity dispersion, which vary with distance from the SMBH. We describe the velocity dispersion of objects using:

$$\sigma = \sqrt{\frac{GM_{\bullet}}{(\alpha + 1)r}} \quad (1)$$

where M_{\bullet} is the mass of the SMBH and r is the distance from the SMBH. The velocity dispersion also weakly depends on α , the slope of the density profile, described below.

The number density of the BHs depends on the interplay of different dynamical processes and interactions with other objects. Generally, the number density profile of objects can be described by a power law, $n \propto r^{-\alpha}$. For a single-mass population, the objects will eventually settle onto an equilibrium distribution with $\alpha = 1.75$ (Bahcall & Wolf 1976). In a population with a spec-

trum of masses, the heavier objects tend to sink towards the SMBH due to energy equipartition. We adopt density profiles for a two-component population, BHs and relatively lighter stars, inspired by work in the literature (Aharon & Perets 2016; Linial & Sari 2022). The number density of the BHs depends on distance from the SMBH. We use the BH density profile calculated using a Fokker-Plank model in Aharon & Perets (2016), their figure 1 upper left panel. While they consider a four component population (main-sequence stars, BHs, white dwarfs, and neutron stars), their BH cusp is comparable to the analytic result for a two-component population from Rom et al. (2024a) in the inner 0.1 pc region of the NSC. We note that they do diverge outside of this region, but as the dynamical processes operate on long (> 10 Gyr) timescales outside of 0.1 pc, it will not significantly change our results. The profile yields $\gtrsim 1000$ BHs in the inner 0.1 pc of the NSC, consistent with our choice to follow 1000 BHs in this region.

Most models predict that the relatively lighter stars should lie on a shallower cusp with index $\alpha \lesssim 1.5$ (eg. Bahcall & Wolf 1976; Alexander & Hopman 2009; Pretor & Amaro-Seoane 2010; Linial & Sari 2022). However, collisions between the stars themselves can deplete the stars (Mastrobuono-Battisti et al. 2021; Rose et al. 2023; Sidhu et al. 2025; Kim & Goodman 2026), and observations of the Milky Way’s nuclear star cluster have indicated a range of α between roughly 1.1 and 1.4 (Habibi et al. 2019; Schödel et al. 2020). For the stellar density, we use:

$$\rho = \rho_0 \left(\frac{r}{r_0} \right)^{-\alpha} \quad (2)$$

where r is the distance from the SMBH in pc, r_0 is a normalization value in pc, and α is the density slope. We adopt $r_0 = 0.25$ pc and $\rho_0 = 1.35 \times 10^6 M_\odot \text{ pc}^{-3}$ to normalize the power-law (Genzel et al. 2010) and $\alpha = 1.25$ for the slope of the profile. Our rational for the value of α is that this choice can only lead to a lower star-BH collision rate due to a lower stellar density, and therefore a more conservative estimate of BH growth through this channel. We do consider one model with $\alpha = 1.75$, used to give an upper limit on the collision rate and its effects, in the Appendix.

3. BLACK HOLE INITIAL PROPERTIES AND BINARITY

We use sets of initial conditions based on Hoang et al. (2018). While we treat a population of single BHs around the SMBH, it is plausible that some of the BHs initially resided in binaries. We distinguish these binaries as primordial systems, meaning they are the end products of stellar binary evolution as opposed to dy-

namically formation. Any binary system in the central parsec of the Galactic center will experience coherent gravitational perturbations from the SMBH. The SMBH can torque the binary’s orbit and induce binary mergers (for a review of the EKL mechanism, see Naoz 2016). The combination of this effect and mergers from GW emission alone, based on the initial binary configuration, can lead to roughly 15% of BH binaries merging within the NSC (Hoang et al. 2018). Binaries in the NSC are also subject to frequent weak gravitational interactions with other surrounding stars, and in a process called binary evaporation, these interactions can unbind some of the binaries (e.g., Heggie 1975; Stephan et al. 2016; Rose et al. 2020). Hoang et al. (2018) study a population of BH binaries within the sphere of influence of the SMBH self-consistently. We therefore account for the presence of primordial binaries as 15% of the BH population, using their final conditions as our initial conditions.

We consider two cases for BH initial mass and spin distributions. In the first case, we use the same initial mass distribution as Hoang et al. (2018), but assume all the BHs were single from birth and have zero initial spin. In the second case, we compute the final masses and spins (see Section 4.1 for equations) of the merger products from Hoang et al. (2018) and combine them with their single BHs from the unbound primordial binaries. The overwhelming majority of their primordial binaries either merge or become unbound within < 1 billion year, making the single BH population a reasonable starting condition for our ~ 10 billion year timescale simulation. We note that they also have a subset of primordial binaries that neither merge nor become unbound. These systems constitute $\lesssim 40\%$ of their initial systems, and at the end of their simulations, single BHs outnumbered binaries by about 2.5 to 1, meaning the population of BHs at later times should be dominated by singles. As dynamical processes related specifically to binary systems, such as binary-single interactions, are beyond the scope of this study, we reserve the inclusion of these systems for future work.

Hoang et al. (2018)’s initial mass distribution extends up to $\sim 90 M_\odot$. In addition to the first two sets of initial mass and spin distributions described above, we also consider a more conservative lower limit BH mass distribution based on Cluster Monte Carlo (CMC) globular cluster simulations by Kremer et al. (2020) (see also, Belczynski et al. 2016). We assume solar metalliticy for all stars. Similar to above, we have one set of initial conditions where all BHs are single and non-spinning and another set where a subset of the BHs are the products of primordial mergers. Specifically, we take our lower limit mass distribution and randomly pair and merge

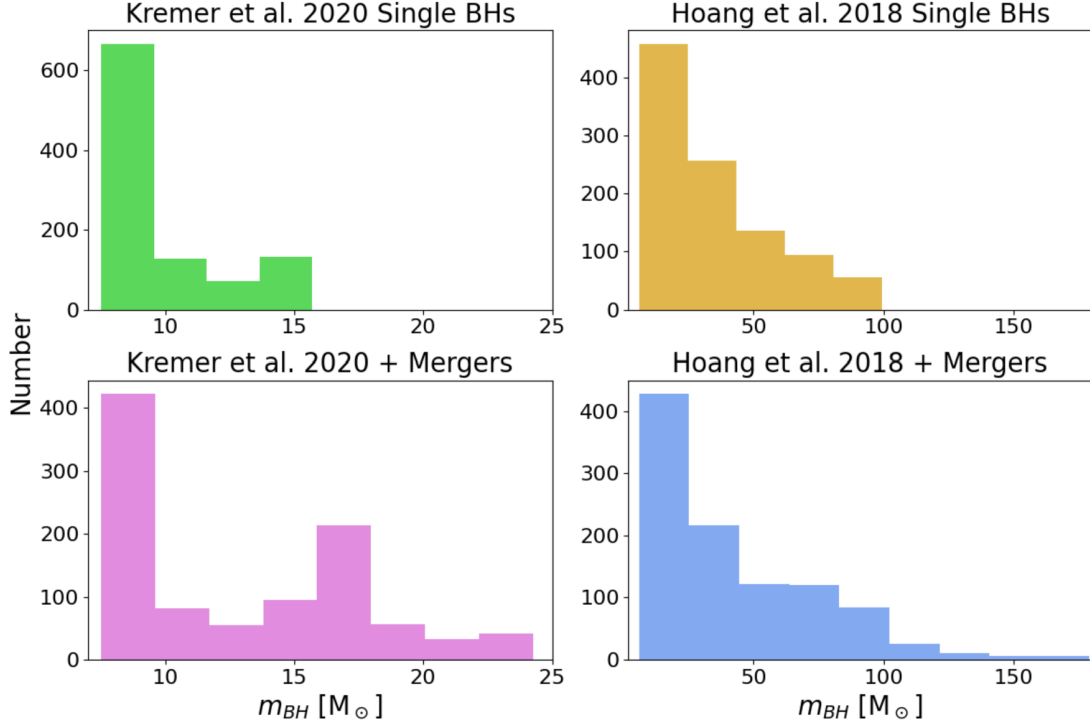


Figure 1. We show the distributions for the four initial BH mass distributions described in Section 2.1. **Left:** The lower limit refers to the conservative case of all initially low mass stellar BHs from Kremer et al. (2020); Belczynski et al. (2016), as well as the lower limit where 30% of the binary BHs have primordial mergers. **Right:** The upper limit describes a case that includes primordial binaries and single BHs. The right top panel describes a case where BHs are evaporated describes a mass distribution of all initially single BHs from Hoang et al. (2018).

15% of the BHs so that the same fraction have had a previous primordial BH-BH merger, either EKL-induced or through GW emission alone, as in the simulations of Hoang et al. (2018). While GW merger rate can depend on BH mass (see Hoang et al. 2018), we hold the fraction of merged systems fixed for a direct comparison of initial conditions. The probability density functions of these four distributions are shown as histograms in Figure 1. We see that the upper limit, including mergers, allows for BH mass as high as $175 M_{\odot}$, while our lower limit only extends to $25 M_{\odot}$. While we do not show the initial spin distributions in Figure 1, the initial conditions with mergers have a peak around 0.7, consistent with (e.g., Borchers et al. 2025; Fishbach et al. 2017; Tagawa et al. 2021; Gerosa & Fishbach 2021; Antonini et al. 2019; Mai et al. 2025). The initial spin distributions can be seen in Figure 3, where we discuss their evolution over the course of the simulations.

4. MODELING PHYSICAL PROCESSES WITHIN THE CLUSTER

We account for a number of dynamical processes in tandem within the cluster using a statistical approach. Each physical process in the cluster has an associated timescale, which in turn depends on the stellar density

profile and velocity dispersion. We describe our treatment of the stellar dynamics below.

4.1. Gravitational Wave Capture Between Single Black Holes

BH-BH binaries form from GW emission from close encounters between single BHs. During these close encounters, the BHs must radiate enough energy away through GWs to become a bound system (e.g., Quinlan & Shapiro 1987; O’Leary et al. 2009). The maximum impact parameter to produce a merger is b_{max} :

$$b_{max} = \left(\frac{340\pi\eta}{3} \right)^{1/7} \frac{GM_{tot}}{c^2} \left(\frac{v_{rel}}{c} \right)^{-9/7}, \quad (3)$$

where M_{tot} is the total mass of the two compact objects, η is their symmetric mass ratio, $\eta = m_1 m_2 / (m_1 + m_2)^2$, and v_{rel} is relative velocity at infinity, which we take to be the velocity dispersion given by Eq. 1 (O’Leary et al. 2009; Gondán et al. 2018; Hoang et al. 2020). We note that there is also a minimum impact parameter, b_{min} ,

$$b_{min} = \frac{4GM_{tot}}{c^2} \left(\frac{v_{rel}}{c} \right)^{-1}, \quad (4)$$

for which any interaction with $b < b_{min}$ will be a direct collision. Therefore, the GW capture cross section is:

$$A_{cap} = \pi(b_{max}^2 - b_{min}^2) \quad (5)$$

(e.g., Hoang et al. 2020). While direct collisions between BHs still result in a merger, the cross-section as set by b_{min} is so small that including or excluding these interactions does not change our results. With the cross-section for interaction, the timescale for GW capture can be calculated as:

$$t_{GW} = (A_{cap} n_{BH} \sigma)^{-1}, \quad (6)$$

where n_{BH} is the number density of BHs.

For each BH in our sample population, we estimate the timescale for GW capture from Eq. 6 by evaluating n_{BH} and σ at the BH's semimajor axis about the SMBH. We take m_2 in η to be the average of the initial mass distribution. The probability of GW capture occurring over an interval of time Δt is $\Delta t / t_{GW}$. For choice of Δt , the integration timestep, see Section 4.2. After determining the GW capture probability, we generate a random number between 0 and 1. If the number is less than or equal to the capture probability, we assume a GW capture has occurred (emulating the methodology in Rose et al. 2022). Once we have determined statistically that GW capture has occurred, we draw a mass and spin for the second BH from the initial distribution. Calculations from O'Leary et al. (2009) indicate that BH binaries formed through GW capture in NSCs form with high eccentricity and merge rapidly, before the BH binary can be dynamically affected by a passing object. Therefore, we assume the merger is prompt, within hours of the binary's formation. We then calculate the final mass, spin, and recoil kick using the same equations as the Cluster Monte Carlo Code (e.g., Rodriguez et al. 2022), which are drawn from numerical relativity and other studies (e.g., Barausse et al. 2012; Barausse & Rezzolla 2009). Specifically, final merger remnant mass is determined by:

$$\frac{M_f}{M_{tot}} = 1 - \eta(1 - 4\eta)(1 - E_{ISCO}) - 16\eta^2 (p_0 + 4p_1\chi_{\parallel}(\chi_{\parallel} + 1)) \quad (7)$$

where $E_{ISCO} = \sqrt{1 - 2/3r_{ISCO}}$ and the fitting constants are $p_0 = 0.04827$ and $p_1 = 0.01707$ (Reisswig et al. 2009; Barausse et al. 2012; Rodriguez et al. 2018). ISCO refers to the innermost stable circular orbit of matter accreting into the BH. χ_{\parallel} is the parallel component of the initial spin parameter, χ . This parameter is normalized by J/M^2 , where J is the angular momentum and M is the mass of the system (Li & Bambi 2014). χ_{\parallel} is defined as:

$$\chi_{\parallel} = \frac{m_1^2\chi_1 + m_2^2\chi_2}{(m_1 + m_2)^2} L \quad (8)$$

for BHs with masses m_1 and m_2 and spins χ_1 and χ_2 . Given L , the orbital angular momentum, we also calculate the final spin as:

$$\chi_f = \min \left(1, \left| \frac{q^2\chi_2 \cos \theta_2 + \chi_1 \cos \theta_1}{(1+q)^2} + \frac{qL}{(1+q)^2} \right| \right) \quad (9)$$

where q is the mass ratio, $\cos \theta_1 = \chi_1 L$, and $\cos \theta_2 = \chi_2 L$.

r_{ISCO} is defined as:

$$r_{ISCO} = 3 + Z_2 \mp \sqrt{(3 - Z_1)(3 + Z_1 + 2Z_2)}, \quad (10)$$

where Z_1 and Z_2 are parameters dependent on χ :

$$\begin{aligned} Z_1 &= 1 + (1 - \chi^2)^{1/3}[(1 + \chi)^{1/3} + (1 - \chi)^{1/3}] \\ Z_2 &= [3\chi^2 + Z_1^2]^{1/2}. \end{aligned} \quad (11)$$

4.1.1. Recoil kicks

Depending on asymmetries in the system, GW radiation can be preferentially beamed in a particular direction, imparting a recoil kick on the merger product. We account for the dynamical effects of this recoil kick as follows. First, we begin by computing the components of velocity kick using equations from e.g., Holley-Bockelmann et al. (2008)

$$v_{kick} = (1 + e)[x(v_m + v_{\perp} \cos \xi) + yv_{\perp} \sin \xi + zv_{\parallel}], \quad (12)$$

where

$$v_m = A \frac{q^2(1-q)}{(1+q)^5} \left(1 + B \frac{q}{(1+q)^2} \right), \quad (13)$$

$$v_{\perp} = H \frac{q^2}{(1+q)^5} (\chi_{\parallel,2} - q\chi_{\parallel,1}), \quad (14)$$

$$v_{\parallel} = K \cos(\Theta - \Theta_0) \frac{q^2}{(1+q)^5} (\chi_{\perp,2} - q\chi_{\perp,1}), \quad (15)$$

and Θ refers to the angle of the direction of the merger, Θ_0 refers to the angle of the initial direction of motion, and ξ refers to the angle resulting from the unequal mass and spin contributions in the recoil kick. For each merger, these angles are chosen according to a uniform distribution, and the fitting constants, A, B, H , and K can be found in Holley-Bockelmann et al. (2008) (see also, e.g., Campanelli et al. 2007; González et al. 2007; Lousto & Zlochower 2008; Lousto et al. 2012; Gerosa & Moore 2016). We apply the kick instantaneously at some point along the binary black hole's orbit about the SMBH. We draw the location of the merger statistically,

weighted by the time spent at each point along the orbit. We calculate the new orbit of the BH merger product about the SMBH from the new mass and velocity vector of the merger product (similar to applications of various types of kicks in Naoz et al. 2022; Hoang et al. 2022; Jurado et al. 2024; Rose & Mockler 2025).

4.2. Direct Collisions with Stars

Direct collisions with stars can occur in NSCs. Each BH is expected to collide with stars over a characteristic timescale, the collision timescale:

$$t_{\text{coll}} = \frac{1}{nA\sigma}, \quad (16)$$

where n_{\star} is the number density of stars, A is the cross-section of interaction, and σ as the velocity dispersion. The cross-section of interaction, A , is the geometric cross-section plus a term for gravitational focusing. The collision timescale becomes:

$$t_{\text{coll}}^{-1} = \pi n \sigma \times \left(f_1(e_{\bullet}) r_c^2 + f_2(e_{\bullet}) r_c \frac{2G(m_{\text{BH}} + M_{\odot})}{\sigma^2} \right) \quad (17)$$

where G is the gravitational constant and r_c is the sum of the radii of the interacting objects, a black hole with mass m_1 and a star with mass $1 M_{\odot}$. As described in Rose et al. (2020), $f_1(e_{\bullet})$ and $f_2(e_{\bullet})$ account for the effect of the BH's orbital eccentricity e_{\bullet} about the SMBH on the collision timescale, while n and σ are calculated from Eq. 2 and 1 at the semimajor axis of the orbit. We assume the stars in the NSC are a uniform population of $1 M_{\odot}$ stars such that $n_{\star} = \frac{\rho}{M_{\odot}}$ where ρ is the stellar density profile, described by a power law (see Eq. 2). The probability of a collision occurring over the integration timestep is $\Delta t / t_{\text{coll}}$. We initially set Δt to be 10^6 years (for discussion, see Rose et al. 2022), however we adjust the timestep during the simulation always be less than the collision timescale. Similarly to Section 4.1 with GW capture, after the determining the collision probability, we generate a random number between 0 and 1. If the number is less than or equal to the collision probability, we assume a collision has occurred.

4.2.1. Mass Growth through Collisions

BHs may accrete mass during a direct collision with a star. Following each collision, we adjust the mass of the BH following Rose et al. (2022). First, we estimate the amount of mass captured by the BH from the star based on Bondi-Hoyle accretion:

$$\dot{m} = \frac{4\pi G^2 m_{1,i}^2 \rho_{\star}}{(c_s^2 + \sigma^2)^{3/2}}. \quad (18)$$

where $m_{1,i}$ is the BH's initial mass, ρ_{\star} is the star's density, and c_s is the speed of sound within the star (g.g., Bondi & Hoyle 1944; Bondi 1952; Shima et al. 1985; Edgar 2004). We approximate ρ_{\star} as $\frac{3M_{\odot}}{4\pi R_{\odot}^3}$ and take $c_s = 600 \text{ km s}^{-1}$ as the sound speed (Christensen-Dalsgaard et al. 1996). The amount of mass that the BH manages to capture from the star can then be approximated as:

$$m_{\text{cap}} = \min(\dot{m} \times t_{\star, \text{cross}}, 1 M_{\odot}), \quad (19)$$

where $t_{\star, \text{cross}} \sim R_{\star}/\sigma$ is the crossing time of the BH within the star. While the BH can capture mass from the star through direct collisions, radiative feedback can prevent it from accreting all of the stellar material. We estimate the accreted mass to be a factor $v_{\text{esc}}/(c\eta)$ less than the captured mass, where v_{esc} is the escape velocity from the BH at $1 R_{\odot}$ and $\eta = 0.1$ is the accretion efficiency at the ISCO (see Rose et al. (2022) for more details and discussion of the accretion). We then adjust the BHs mass by $\Delta m = m_{\text{cap}} \times v_{\text{esc}}/(c\eta)$.

4.2.2. Spin Change through Collisions

The spin of a BH also changes following a collision with a star due to angular momentum conservation during the accretion process. We use equations from Volonteri et al. (2013) to calculate the final spin of the BH, represented by χ . The final spin χ_f of the BH is:

$$\chi_f = \begin{cases} \frac{r_{\text{ISCO}}^{1/3}}{3} \cdot \frac{m_{1,i}}{m_{1,f}} \left(4 - \sqrt{\left(\frac{3m_{1,i}^2 r}{m_{1,f}^2} \right)} - 2 \right), & \text{if } \frac{m_{1,f}}{m_{1,i}} \leq r^{1/2}, \\ 1, & \text{if } \frac{m_{1,f}}{m_{1,i}} \geq r^{1/2}. \end{cases} \quad (20)$$

where $\frac{m_{1,f}}{m_{1,i}}$ is the percent change in mass of the BH, and r_{ISCO} is defined in Equation (10).

4.3. Relaxation and Dynamical Friction

The orbital energy of a BH in a NSC changes over time through weak gravitational interactions with other objects. This process acts over the associated two-body relaxation timescale, which describes the time for the orbital energy and angular momentum to change by order of themselves:

$$t_{\text{relax}} = 0.34 \frac{\sigma^3}{G^2 \rho \langle M_{\text{avg}} \rangle \ln \Lambda}. \quad (21)$$

$\ln \Lambda$ is the Coulomb logarithm and $\langle M_{\text{avg}} \rangle$ is the average object mass and ρ is their mass density (e.g., Binney & Tremaine 2008). Occasionally, weak gravitational interactions cause BHs to wander too close to the SMBH, which eventually leads to inspiral into the SMBH and GW emission, an event known as an Extreme Mass Ratio Inspiral (EMRI) (Magorrian & Tremaine 1999; Wang

& Merritt 2004; Hopman & Alexander 2005; Aharon & Perets 2016; Stone & Metzger 2016; Amaro-Seoane 2018; Sari & Fragione 2019; Naoz et al. 2022). We model the relaxation process by simulating a random walk in the semimajor axis and eccentricity parameter space (for the full equations, see Naoz et al. 2022; Rose et al. 2022).

GW recoil kicks can also alter the orbit of the BH about the SMBH. Depending on the strength of the kick and the BH’s initial orbit, the merger product can be ejected from the inner 0.1 pc of the cluster. If the merger product’s new orbit remains bound to the SMBH, we allow it to sink back into the inner 0.1 pc over a mass-segregation timescale:

$$t_{\text{seg}} \approx \frac{M_{\text{star}}}{m_{\text{BH}}} \times t_{\text{relax}}(M_{\text{avg}} = M_{\text{star}}, \rho = \rho_{\text{star}}) \quad (22)$$

(Spitzer 1987; Fregeau et al. 2002; Merritt 2006). This treatment of dynamical friction is consistent with previous semianalytic models of successive BH-BH mergers in NSCs (as has been done in, e.g., Antonini & Rasio 2016; Fragione et al. 2021). If the merger product is ejected from the cluster, it triggers a stopping condition in our code and we record the final mass and orbital configuration.

4.4. Gravitational Wave Inspiral into the SMBH

We also account for GW dissipation between each cluster BH and the SMBH. We calculate changes to the orbital eccentricity and semimajor axis due to GW emission over each timestep using equations from Peters & Mathews (1963); Peters (1964). These changes become particularly important within $\sim 10^4$ AU of the SMBH, where the inspiral timescale is roughly less than simulation time of 10 billion years.

5. RESULTS

We run four sets of simulations of 1000 BHs each embedded in a NSC composed of other BHs and $1 M_{\odot}$ stars, as described in Sections 2 and 4. We list the simulations and their initial conditions in Table 1. We discuss the results and implications below.

5.1. Effect of Sequential Collisions with Stars on Black Hole Spin

We begin by isolating the effect of successive BH-star collisions on the BHs by running a simulation without any GW capture. We use the Hoang et al. (2018) Single BHs initial conditions (gold). We evolve BH spin from collisions with stars using the equations described in Section 4.2.2 to account for changes in a BH’s spin due to the accretion of stellar material (e.g., Volonteri et al. 2005; Volonteri et al. 2013; Gammie et al. 2004). In the

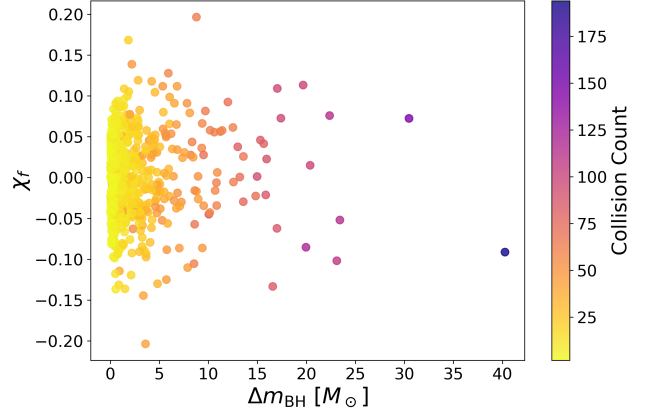


Figure 2. We show the resulting spins and the change in mass of 1000 BHs after 1 billion years with the Hoang et al. (2018) Single BHs (gold) initial conditions, as described in Section 5.1. All BHs underwent at least two collisions with stars, with a maximum number of collisions per BH of 194. As shown in Table 1, after 1 billion years, 2.3% of the population are IMBHs with mass above $\sim 100 M_{\odot}$.

case of multiple accretion episodes, BHs “spin down” when the accretion disk rotates in the opposite direction of the BH’s initial spin, χ_i , while BHs “spin up” if they accrete mass from a disk rotating in the same direction as spin χ_i . A larger Δm_{BH} , or mass accreted, corresponds to a larger change in spin, $\Delta \chi$ (see Equation (20)). However, for the same Δm_{BH} , retrograde accretion leads to a greater magnitude of spin change. When the accretion disk is retrograde with respect to the BH spin, the ISCO is further from the BH and therefore carries more angular momentum than when the accretion disk is prograde. Angular momentum conservation demands a greater change in the BH’s spin upon accreting the material. Therefore, for the same Δm_{BH} , retrograde accretion leads to a greater magnitude spin change.

With each collision, we randomly draw whether the accretion disk is prograde or retrograde with respect to the BH’s initial spin, treating this process as a random walk. We show the final spin parameter versus total change in mass from this simulation in Figure 2. The BHs which experienced the most mass growth from successive collisions have lower spins. Our results are consistent with previous findings related to retrograde accretion (Hughes & Blandford 2003; Volonteri et al. 2005; Volonteri et al. 2013; Kiroğlu et al. 2025b; Borchers et al. 2025), that higher mass BHs have lower spins after many successive mergers. Our simulation achieves this same result for successive collisions in galactic nuclei. We therefore expect IMBHs formed through successive BH-star collisions to be low-spinning, with $\chi < 0.2$.

Table 1. A summary of black hole growth and merger properties across our simulations. In the second column, we indicate the slope of the stellar density profile, α , used for the simulation. The merger column tallies the total number of BH-BH captures that occur over the simulation, with the exception of gold*, which refers to the simulation with gold initial conditions that only considers stellar collisions with no GW capture. We note that some of these captures can occur to the same BH, leading to multiple generations of mergers. We also show the maximum BH mass and spin achieved in each of our simulations, as well as the number of BHs that double in mass, grow by an order of magnitude, and grow by two orders of magnitude. Most notably, the last two simulations with GW capture produced IMBHs, as well as the stellar collisions-only simulation. We note that a small fraction of BHs were initially IMBHs ($> 100 M_\odot$) in the blue case.

IC	Stellar Profile	Mergers	Max Mass BH [M_\odot]	Max Spin BH	BHs $> 2 \times M_i$	BHs $> 10 \times M_i$	% BHs $> 100 M_\odot$
Green	$\alpha = 1.25$	34	28.4	0.712	8	0	0
Pink	$\alpha = 1.25$	40	80.5	0.894	13	0	0
Gold	$\alpha = 1.25$	371	407.3	0.805	79	4	7.8%
Blue	$\alpha = 1.25$	535	526.0	0.855	103	8	14.3%
Gold*	$\alpha = 1.25$	N/A	123.7	0.196	0	0	2.3%

5.2. Retention of Merger Products

The magnitude of a GW recoil kick depends in part on the mass ratio of the merging BHs and their spins. While we assume all BHs are initially non-spinning, stellar collisions can modify the spins of these BHs. We find that $\sim 92\%$ of single BHs have non-zero spins prior to a GW merger due to collisions with stars; however, the magnitude of $\Delta\chi$ from stellar collisions is low, as shown in Figure 4. We can understand where GW recoil kicks become important by comparing its characteristic speed to the orbital speed as a function of distance from the SBMH. For low-spinning BHs ($\chi < 0.1$), typical kick speeds are between 0 and ~ 200 km/s for a range of mass ratios. The Keplerian speed exceeds ~ 100 km/s within about 0.03 pc. As expected, all of our merger products are retained in this steep potential. In fact, none of recoil kicks changed the semi-major axis of the BH's orbit by more than an order of magnitude. However, we note that the orbital eccentricity can increase the recoil speed. Sopuerta et al. (2007) found this increase to be a factor of $1 + e$, while numerical relativity studies indicate that an eccentric orbit can boost the recoil speed as much as 25% (Sperhake et al. 2020; Radia et al. 2021). GW bremsstrahlung produces eccentric systems (e.g., Rom et al. 2024b). In the most eccentric case, the kick speed could be a factor of 2 larger. While NSCs should still be able to retain a large fraction of merger products, we reserve a more complete exploration of the effect of BH birth spins and orbital eccentricity on the retention fraction for future work.

5.3. Comparing Initial and Final Mass and Spin Distributions

Figure 3 shows the final vs. initial BH mass and spin distributions from our simulations. In order to understand the mass growth of the BHs, we can compare the maximum final mass to the maximum initial mass from

the distributions. For initial conditions with primordial mergers, the initial maximum BH mass is roughly a factor of 2 higher than all initially single BHs. Primordial mergers therefore lead to more mass growth for the BH population overall. As can be seen in Table 1 and Figure 3, more BHs double in mass over the course of the simulation for initial conditions with previously merged BHs from primordial binaries. However, the maximum mass has the same order of magnitude. Both lower limit cases (pink and green) resulted in similar scales of mass growth for the BHs, while the same is true for the both upper limit distributions. The lower limit mass distribution leads to a maximum final BH mass of 28.4, versus $80.5 M_\odot$ with primordial mergers. The upper limit initial mass distribution with and without primordial mergers lead to maximum masses of 407.3 versus $526.0 M_\odot$, respectively.

For each BH in our sample, we show its change in mass from capture of other BHs versus direct collisions with stars in Figure 4. The mass growth of the sample BHs comes primarily from GW capture of other BHs, as opposed to accretion from stars during direct collisions. Even though BH-star collisions are more frequent, the mass accreted from these interactions is kept low due to our prescription to estimate mass loss through feedback. We attribute the dependence of the mass growth and merger rate of the BHs on the initial BH mass distribution to the fact that the BH-BH GW capture timescale is roughly proportional to $1/m_{BH}^2$.

Without primordial mergers, all BHs are initially non-spinning, while the population with primordial mergers includes BHs with spins less than 0.7. However, the final spin distributions for all cases show a more continuous distribution. For the lower limit cases, which experienced less GW mergers and accrete less mass from stars, there is a sharper peak at about 0.7. Contrastingly, for the upper limit cases that experience more mass growth

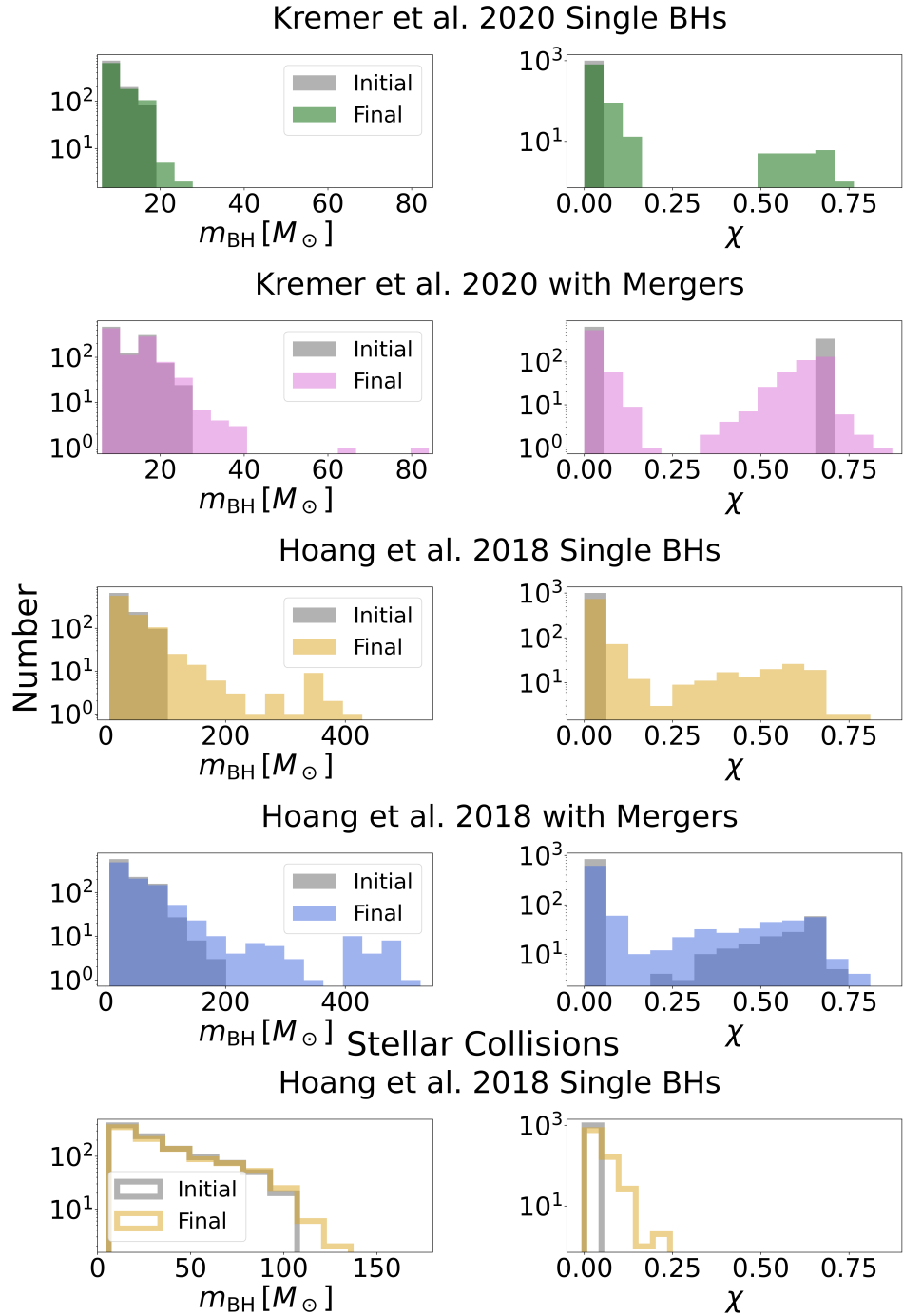


Figure 3. **Left:** We plot the distributions of initial mass in gray and final mass in color for the four initial conditions described in Section 3, as well as IC gold (Hoang et al. (2018) Single BHs) with only stellar collisions with density $\alpha = 1.25$. **Right:** We plot the distributions of initial spin in gray and final spin in color for the four initial conditions described in Section 3.

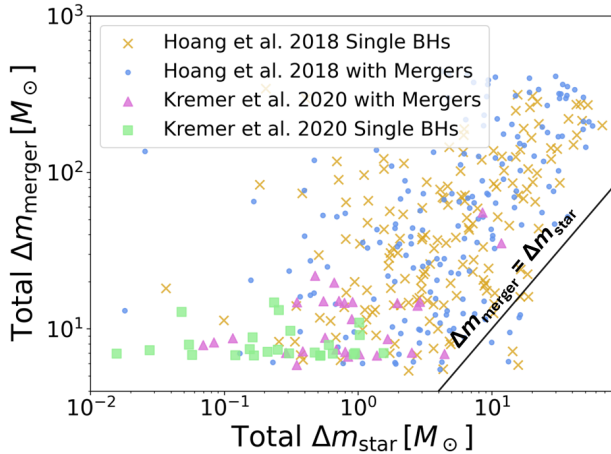


Figure 4. Contribution of each dynamical channel to that mass growth for each BH with $M_f > M_i$. The x-axis shows the amount of mass accreted over the entirety of the simulation from direct collisions with stars, which is limited by both feedback during the accretion process and environmental conditions like stellar density and velocity dispersion. The y-axis shows the growth through BH-BH gravitational wave capture. For all four sets of simulations, most mass growth for the BHs came from GW capture. To guide the eye, we plot a line in black showing where the change in mass from BH-BH mergers and BH-star collisions are equal.

through mergers and collisions with stars, the distribution appears almost uniform between $\chi = 0.25$ and 0.7 , with a less sharp peak at 0.7 . All distributions exhibit a spread of low-spinning BHs within $\chi \lesssim 0.2$, a signature of accretion of material during many successive collisions with stars.

To highlight the difference between stellar collisions-only and GW mergers in mass and spin distributions, in the last row of Figure 3 we plot a simulation using Hoang et al. (2018) Single BHs (gold) initial conditions and including only collisions with stars on a $\alpha = 1.25$ density profile. Figure 4 suggests more mass on average is gained through mergers, and this effect is visible in Figure 3 as well. The final mass distribution shows mass accretion through stars, but significantly less overall mass growth than the other simulations with GW mergers. Additionally, the spin peak at 0.7 , a hallmark of GW mergers, is not present for the stellar collision-only simulation, whereas the diminishing spin over successive collisions, as in Figure 2, is present. As shown in the last row of Table 1, IMBHs represent $\sim 2\%$ of the population, but this is largely the result of the high mass initial distribution.

5.4. IMBH Formation

We assess whether any BHs in our sample population experience significant enough mass growth to become

IMBHs, defined as a BH with mass $> 100 M_\odot$. We note that our upper limit mass distribution with single BHs extends up to but does not exceed $100 M_\odot$. However, with primordial mergers, the Hoang et al. (2018) with Mergers (blue) initial conditions already contain IMBHs by this definition. As apparent in Figure 3, the lower limit mass distributions do not result in any IMBHs with $\alpha = 1.25$ for the stellar cusp. The steepness of the stellar cusp can affect the mass growth of the BHs because it controls the number density of stars with which the BHs can collide. Previously, Rose et al. (2022) showed that BH-star collisions alone can produce $\sim 100 M_\odot$ IMBHs with Bahcall-Wolf profile ($\alpha = 1.75$) for the stars. However, for the initial conditions that we sample in this study, only the upper limit initial mass distributions, with and without primordial binaries, consistently produce IMBHs. Crucially, our results indicate that the upper limit initial conditions can produce IMBHs from either sequential BH mergers or successive BH-star collisions alone. Specifically, IMBHs represent 14.3% (7.8%) of the final population for the blue (gold) initial distribution, as shown in Table 1. In other words, both channels working in concert with one another are not necessary to produce IMBHs. We note that IMBHs grown solely through successive BH-star collisions tend to end up with lower spins than those formed through BH-BH mergers. This trend is partly driven by our simplified spin prescription for BH-star collisions, which assumes fully anti-aligned accretion during spin-down and therefore represents a lower limit on the resulting spin distribution. We reserve the exploration of other initial conditions and cluster properties for future work, such as whether there is a mass distribution between our lower and upper limits that consistently produces IMBHs.

The most massive BH formed across all of our simulations was $526 M_\odot$. As a BH becomes significantly more massive than the rest of the population, it begins to sink towards the SMBH due to dynamical friction until it becomes an EMRI. All BHs with final mass $> 400 M_\odot$ become EMRIs. Furthermore, for gold (blue) initial conditions, 70% (55%) of BHs over $> 200 M_\odot$ became EMRIs. These events still have mass ratio $< 10^{-3}$ with the SMBH and therefore do not meet the criterion for intermediate mass ratio inspirals (IMRIs). However, they may be a signature of efficient dynamical formation of IMBHs in galactic nuclei. These heavier EMRIs occur at later times within the cluster, after dynamical formation channels like GW capture have had time to act and produce IMBHs through sequential mergers. The rate of EMRIs with mass ratio $> 5 \times 10^{-5}$ is approximately 4 Gyr^{-1} per Milky Way-like galaxy, and

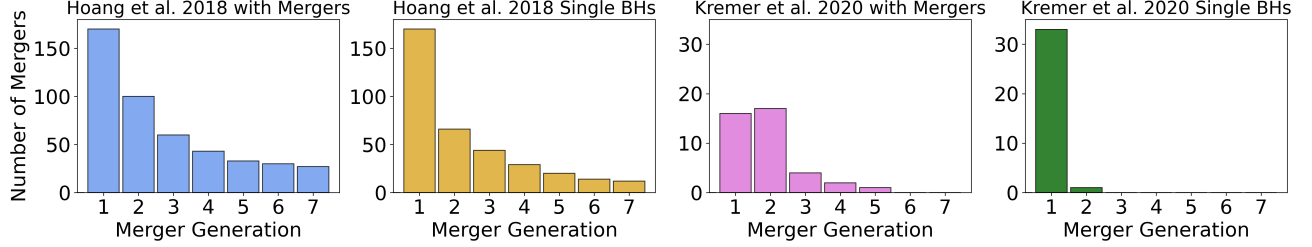


Figure 5. For four simulations described in Table 1, number of mergers from GW capture per highest generation of BH in the event. In calculating the generation of the BH, we account for both previous GW captures in the simulation and primordial mergers from the initial conditions. We find that primordial binaries increases the merger rate with 2G BHs. The initial masses of the BHs seem to have the strongest effect on the number of higher generation mergers. We only show merger generations up to 7G, but the shape can be extrapolated to 7G+ mergers. The highest generation merger was 16G (12G) for blue (gold).

they predominantly occur after ~ 2 Gyr in the simulation. EMRIs with mass ratio $> 1 \times 10^{-4}$ predominantly occur after 4 Gyr in the simulation at a similar rate of 4.8 Gyr^{-1} per galaxy. For the range of initial conditions and cluster parameters explored in this study, IMBHs with masses $> 10^4 M_{\odot}$ cannot form in situ in a NSC, though they may instead be deposited in the NSC through other means, such as an infalling globular cluster (e.g., González Prieto et al. 2025). We note as a caveat on these results that our simulations assume a density profile for the background BHs and stars that are held constant for the entirety of the simulation. We do not account for the effects of an IMBH scattering the relatively lighter BHs and stars to wider orbits as it sinks towards the SMBH (e.g., Baumgardt et al. 2006; Löckmann & Baumgardt 2008). The formation of an IMBH may temporarily suppress the ability of dynamical channels to form another IMBH until the cusp has been replenished (estimated to be on $\gtrsim 50$ Myr timescales for the stars by aforementioned studies).

5.5. Implications for GW Sources

From Figure 5, we can estimate a merger rate from GW capture for different BH generations. Kremer et al. (2020) Single BHs (green) initial conditions gives 30 first generation mergers over our simulation time, yielding a rate of a few $\times 10^{-9} \text{ yr}^{-1}$ per galaxy. This value falls within the range previously computed in the literature (O’Leary et al. 2009), where the rate depends on assumptions about the ratio of BHs to stars, BH mass range, and slope of the cusp (O’Leary et al. 2009; Rose et al. 2022; Liu & Lai 2025, Rose et al. in prep.). The second generation mergers, in which one or both of the progenitor BHs is the product of a previous merger, occur at a much lower rate of a few $\times 10^{-10} \text{ per year per galaxy}$. The overall rate of GW capture is the comparable between the two simulations with Kremer et al. (2020) initial conditions. However, with primordial binaries, mergers that contain a second generation BH

represent a significant fraction of the systems. Both the 1G and 2G merger rate is roughly 10^{-9} per year, while mergers that contain a third generation or higher BH occur at a rate of $\sim 5 \times 10^{-10} \text{ per yr}$.

Similarly, we calculate merger rates from GW capture for Hoang et al. (2018) Single BHs (gold) initial conditions. This simulation gives 150 first generation mergers, corresponding to merger rate of 10^{-8} per year per galaxy, which is an order of magnitude higher than the rate for our lower mass limit. Additionally, the 2G merger rate, 5×10^{-9} per year, is also higher than the corresponding rate for the lower mass limit. The first generation merger rate for Hoang et al. (2018) with Mergers (blue) is comparable to the gold rate. However, the blue 2G merger rate is closer to 10^{-8} per year. The qualitative effect of primordial mergers on the merger rate is similar in both the upper and lower limit initial mass distributions: the blue initial conditions resulted in more 2G mergers as well as higher generation mergers. The 2G mergers represent about twice the fraction of total mergers compared to the gold simulation. The rate of mergers for the upper mass limit with a 3G or higher generation BH is at most $\sim 5 \times 10^{-9}$ per year, an order of magnitude higher than the corresponding rate for the lower mass limit.

For all mergers from GW capture, we show the total mass versus the time of merger in Figure 6, color-coded by the generation of BH. Generally, the mergers with the largest masses occur at later times. Mergers with higher generation BHs (3G+) occur predominantly in our upper limit mass distribution simulations. The higher generation, more massive mergers occur ~ 2 Gyr into the simulation. Additionally, higher generation BHs are more likely to occur in any populations with primordial mergers. For mergers with the highest generation BHs (6G+), they occur almost exclusively when the higher generation BH has mass $> 250 M_{\odot}$, shown in Figure 7. Correspondingly, BHs with mass $> 250 M_{\odot}$ are almost exclusively 6G+. The effect of primordial bi-

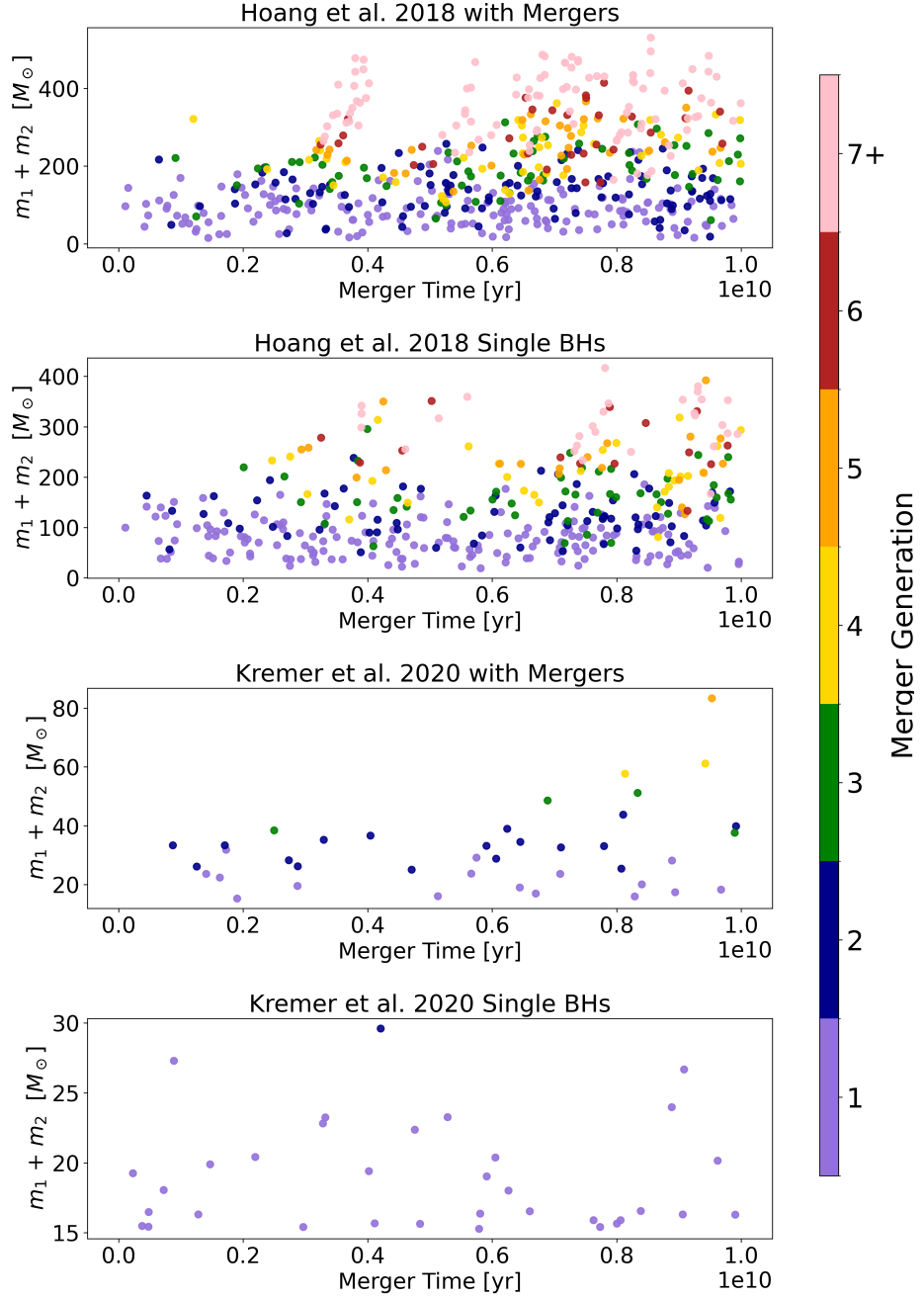


Figure 6. For the four simulations described in Table 1, the sum of the mass of the two merging BHs is shown against the time of the merger. Consistent with Figure 5, the Hoang et al. (2018) populations have higher generation mergers than the lower limit populations. Across all populations, higher generation mergers take place later in the simulation.

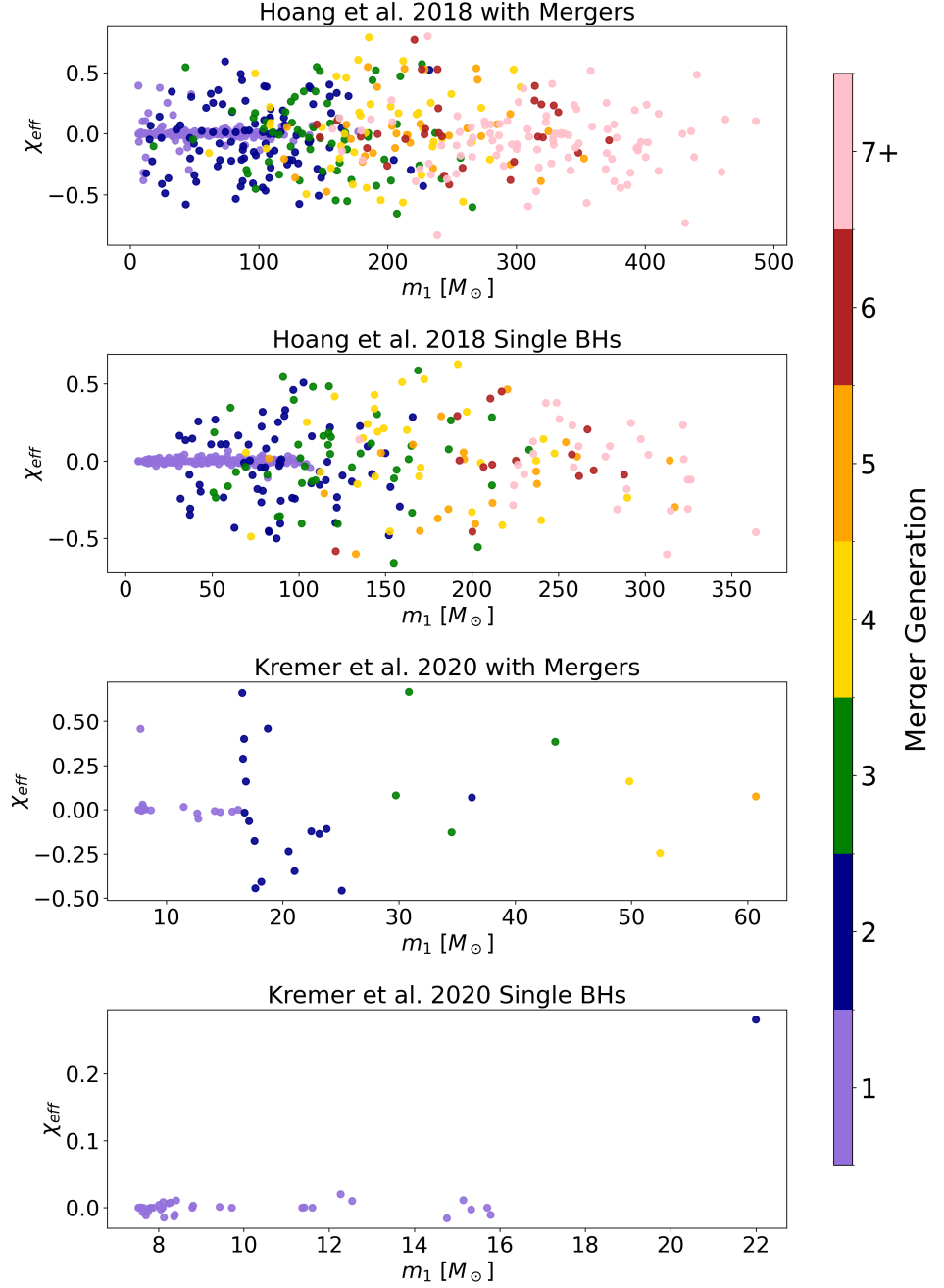


Figure 7. For the four simulations described in Table 1, the resulting χ_{eff} from a merger event is plotted against the initial mass of m_1 . For all populations except the Lower Limit Single BHs, the range of χ_{eff} is approximately -0.5 to 0.5. As m_1 increases, χ_{eff} increases as well, whereas the most massive m_1 in a population have χ_{eff} with less magnitude, consistent with Figure 2. It is noted that any non-zero spins of first generation BHs is due to accretion from stellar collisions. All populations had a high percentage ($\sim 92\%$) of merging BHs with initially non-zero spin due to stellar accretion. For the Lower Limit Single BHs, the first generation BHs had spins approximately zero.

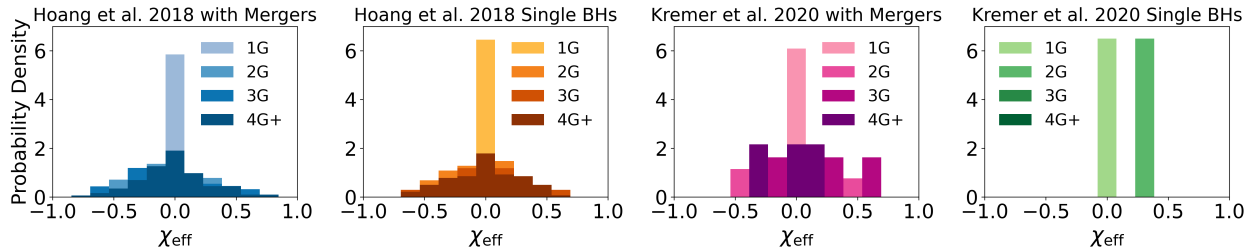


Figure 8. For the four simulations in Table 1, the probability density of χ_{eff} resulting from a merger by GW captures by highest generation BH. We see that for all populations, first generation mergers result in low χ_{eff} . In general, higher generation mergers have larger magnitude χ_{eff} , and the Hoang et al. (2018) populations have larger χ_{eff} than the lower limits.

naries is significant in increasing the number of 2G BHs in the population, and therefore higher generation BHs as well, as described in Section 5.4.

To complement Figure 6, we also show the χ_{eff} of these GW sources in Figures 7 and 8. Specifically, we show the χ_{eff} versus primary mass in Figures 7, color-coded by generation, while Figure 8 shows the χ_{eff} distribution for each merger generation. For all populations other than the last row (Kremer et al. (2020) Single BHs (green) initial conditions), the magnitude of χ_{eff} for successive generation mergers can be $\gtrsim 0.5$. As seen in Figure 7, the magnitude of χ_{eff} tends to decrease with the highest generation mergers, consistent with the results in Section 5.1. Generally first generation mergers have zero initial spin, but considering accretion from stellar collisions, we see some first generation BHs with initially non-zero spin and therefore non-zero, albeit often very small, χ_{eff} .

6. CONCLUSIONS

We consider two channels for modifying the mass and spin distributions of BHs in NSCs:

1. *BH accretion through collisions with stars:* From timescale arguments alone, this channel is the most promising: a BH residing within 10^{-2} pc of the SMBH will experience tens to hundreds of collisions with stars. However, the effect of these sequential collisions on the BHs is limited by the amount the BHs can conceivably accrete from stars during each collision.
2. *BH mergers:* For a population of single BHs, mergers can occur following GW capture. While the timescale for GW capture is much longer than direct BH-star collisions, this process has the advantage of producing appreciable changes in a BH’s mass and spin.

We assess the interplay of these two channels using the semianalytic model described in Section 2. We consider four sets of initial conditions. In two of these initial

conditions, we account for the possibility that a subset of our initial population are the merger products of primordial binaries following Hoang et al. (2018). The first two initial conditions (color-coded as green and pink in Figure 1) adopt lower initial masses for the BHs (for the mass distribution, see Kremer et al. 2020). With primordial mergers (pink), the lower limit extends up to roughly $\sim 30 M_{\odot}$ and has BHs that are initially spinning, while without primordial mergers (green), all BHs are initially non-spinning and have masses extending up to $15 M_{\odot}$. We also test an upper limit mass distribution, which extends to $\lesssim 100 M_{\odot}$ without primordial mergers (gold) and $\lesssim 200 M_{\odot}$ with primordial mergers (blue), as in Hoang et al. (2018). We find the following:

1. **BH Mass and Spin Distributions:** The lower mass limit (green and pink) and upper mass limit (blue and gold) experience similar scales of mass growth, respectively. For the initial conditions with primordial binaries (pink and blue), more BHs within the population grow in mass. However, the most massive final BHs for the green and pink initial distributions have the same order of magnitude, while the same is true for the upper limit blue and gold simulations. The maximum final BH mass from upper limit distributions is an order of magnitude larger than the most massive BH from lower limit distributions. As can be seen in Figure 4, initially more massive BHs experience more mass growth. This is in part because the BH-BH GW capture timescale $\propto \frac{1}{m_{BH}^2}$, while more massive BHs also have a slightly larger cross-section due to gravitational focusing, shortening the collision timescale, and can retain more of a star’s mass during a collision. We conclude that the range of the initial mass distribution is a better predictor the final BH masses than the presence of primordial binaries.
2. **Prospects for Forming IMBHs:** The maximum BH mass produced through dynamical channels in our simulations was about $500 M_{\odot}$. Dy-

namical friction limits the mass of BHs formed in situ to hundreds of M_{\odot} . As the IMBH becomes significantly more massive than other objects in the cluster, it should start sinking towards the SMBH, eventually becoming an EMRI. IMBH formation also depends on the initial mass distribution: IMBHs are not formed at all in the pink and green populations with stellar profile $\alpha = 1.25$.

3. Rate of BH-BH Mergers: We find merger rate is a few $\times 10^{-9}$ per year per galaxy for the lower mass limit (green and pink) assuming a BH density profile from [Aharon & Perets \(2016\)](#). For the upper mass limit (blue and gold), we see a merger rate of an order of magnitude higher, a few $\times 10^{-8}$ per year per galaxy. For 2G mergers, the rates are $\sim 1 \times 10^{-8}$ (blue), $\sim 5 \times 10^{-9}$ (gold), $\sim 1.5 \times 10^{-9}$ (pink), $\sim 1 \times 10^{-10}$ (green). These results demonstrate the significant effect of primordial mergers on the merger rate for the lower mass limit, as the 2G rate for the pink is an order of magnitude higher than the green. Pink contains higher (3G+) generation BHs in mergers; green does not.

4. Other Implications for GW Sources: We find that higher (3G+) generation mergers occur primarily in the upper mass limit and after ~ 2 Gyr. Additionally, the blue population with primordial binaries increase the likelihood of higher generation mergers. The highest generation mergers (6G+) have a primary BH with mass $> 250 M_{\odot}$. For the pink and blue initial distributions, about half of the 2G mergers have either one or both progenitor BHs that was the product of a from primordial binary merger. The expected χ_{eff} depends on the generation of BH. For first generation BHs, the χ_{eff} is approximately zero, though BHs can have non-zero spin as the result of accretion from stellar collisions. For high generation BHs (3G+), the χ_{eff} has magnitude of up to ~ 0.5 . For the highest generation BHs (6G+), χ_{eff} is generally magnitude < 0.5 due to the effect of successive stellar collisions and mergers reducing spin, χ , magnitude.

To understand how populations of single BHs in a NSC evolve over time, we model the effects of BH-BH GW capture and BH-star direct collisions semianalytically. The BH-BH merger rates and properties can depend sensitively on assumptions about the BH masses, initial binary fraction, and density profile within the cluster (see also, e.g., [O’Leary et al. 2009](#); [Liu & Lai 2025](#)). Our work highlights the need to explore the

broad range of initial conditions and assumptions about the cluster in the context of GW source production and IMBH formation.

¹ A.N. was supported by NSF Grant AST-2149425, a
² Research Experiences for Undergraduates (REU) grant
³ awarded to CIERA at Northwestern University. S.C.R.
⁴ thanks the CIERA Lindheimer Fellowship for support.
⁵ F.A.R. acknowledges support from NSF Grants AST-
⁶ 2108624 and AST-2511543. F.K. acknowledges support
⁷ from a CIERA Postdoctoral Fellowship.

⁸ This research was supported in part through the com-
⁹ putational resources and staff contributions provided for
¹⁰ the Quest high performance computing facility at North-
¹¹ western University which is jointly supported by the Of-
¹² fice of the Provost, the Office for Research, and North-
¹³ western University Information Technology.

APPENDIX

To show the effect of stellar density on mass accretion and spin change through stellar collisions, we include two additional simulations with Hoang et al. (2018) single BHs initial conditions, considering only stellar collisions. We include two choices, $\alpha = 1.25$ (shown in the main body of the paper), consistent with our previous four simulations, and $\alpha = 1.75$ for an upper limit, shown here. We see that the choice of α greatly impacts the highest masses formed through stellar collisions, but has a small effect on overall spin change. For $\alpha = 1.75$, masses as high as $\sim 10^7 M_\odot$ were formed, five orders of magnitude higher than the highest mass in the $\alpha = 1.25$ case. While runaway growth is astrophysically interesting, masses as high as these are unrealistic as they would have exhausted the entire supply of stars in the cluster. Our simulation allows for these massive BHs to form because we consider a fixed background population of $1 M_\odot$ stars. However, the majority of the final masses of BHs in the $\alpha = 1.75$ case are comparable with the upper mass limit simulations with GW capture. We reserve the study of the effect of this high stellar density in tandem with GW mergers for future work.

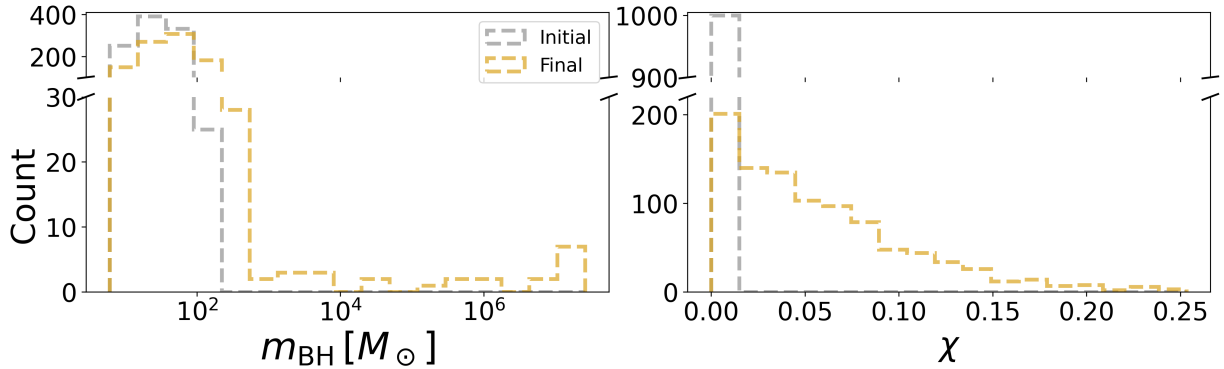


Figure 9. The initial (gray) and final (gold) distributions of mass and spin using gold (Hoang et al. (2018) single BHs) ICs and including only BH-star collisions with stellar density $\alpha = 1.75$.

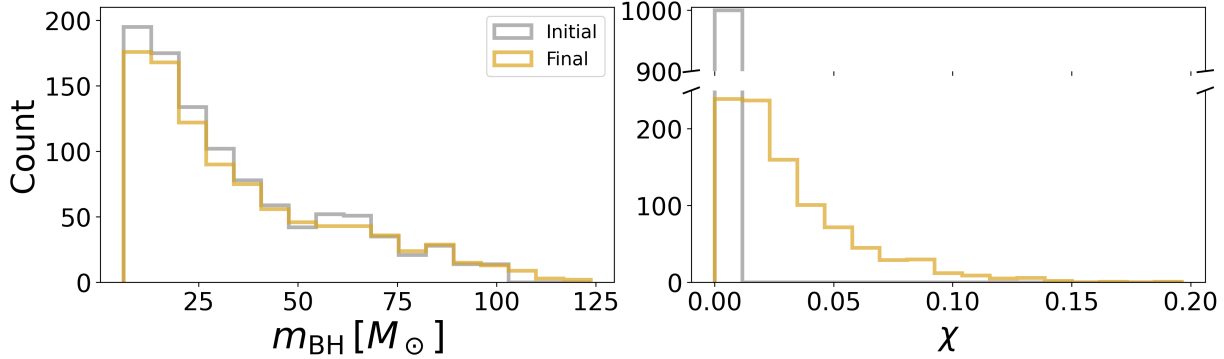


Figure 10. The initial (gray) and final (gold) distributions of mass and spin using gold (Hoang et al. (2018) single BHs) ICs and including only BH-star collisions with stellar density $\alpha = 1.25$.

REFERENCES

Abac, A. G., Abouelfettouh, I., Acernese, F., et al. 2025, *ApJL*, 993, L25, doi: [10.3847/2041-8213/ae0c9c](https://doi.org/10.3847/2041-8213/ae0c9c)

Abbott, R., Abbott, T. D., Abraham, S., et al. 2020, *The Astrophysical Journal Letters*, 900, L13, doi: [10.3847/2041-8213/aba493](https://doi.org/10.3847/2041-8213/aba493)

Aharon, D., & Perets, H. B. 2016, *ApJL*, 830, L1, doi: [10.3847/2041-8205/830/1/L1](https://doi.org/10.3847/2041-8205/830/1/L1)

Alexander, T., & Hopman, C. 2009, *ApJ*, 697, 1861, doi: [10.1088/0004-637X/697/2/1861](https://doi.org/10.1088/0004-637X/697/2/1861)

Amaro-Seoane, P. 2018, *Living Reviews in Relativity*, 21, 4, doi: [10.1007/s41114-018-0013-8](https://doi.org/10.1007/s41114-018-0013-8)

Antognini, J. M., Shappee, B. J., Thompson, T. A., & Amaro-Seoane, P. 2014, *MNRAS*, 439, 1079, doi: [10.1093/mnras/stu039](https://doi.org/10.1093/mnras/stu039)

Antonini, F., Gieles, M., & Gualandris, A. 2019, *Monthly Notices of the Royal Astronomical Society*, 486, 5008, doi: [10.1093/mnras/stz1149](https://doi.org/10.1093/mnras/stz1149)

Antonini, F., & Perets, H. B. 2012, *ApJ*, 757, 27, doi: [10.1088/0004-637X/757/1/27](https://doi.org/10.1088/0004-637X/757/1/27)

Antonini, F., & Rasio, F. A. 2016, *ApJ*, 831, 187, doi: [10.3847/0004-637X/831/2/187](https://doi.org/10.3847/0004-637X/831/2/187)

Bahcall, J. N., & Wolf, R. A. 1976, *ApJ*, 209, 214, doi: [10.1086/154711](https://doi.org/10.1086/154711)

Baibhav, V., Gerosa, D., Berti, E., et al. 2020, *PhRvD*, 102, 043002, doi: [10.1103/PhysRevD.102.043002](https://doi.org/10.1103/PhysRevD.102.043002)

Bailey, V. C., & Davies, M. B. 1999, *MNRAS*, 308, 257, doi: [10.1046/j.1365-8711.1999.02740.x](https://doi.org/10.1046/j.1365-8711.1999.02740.x)

Barausse, E., Morozova, V., & Rezzolla, L. 2012, *The Astrophysical Journal*, 758, 63, doi: [10.1088/0004-637X/758/1/63](https://doi.org/10.1088/0004-637X/758/1/63)

Barausse, E., & Rezzolla, L. 2009, *ApJL*, 704, L40, doi: [10.1088/0004-637X/704/1/L40](https://doi.org/10.1088/0004-637X/704/1/L40)

Baumgardt, H., Gualandris, A., & Portegies Zwart, S. 2006, *MNRAS*, 372, 174, doi: [10.1111/j.1365-2966.2006.10818.x](https://doi.org/10.1111/j.1365-2966.2006.10818.x)

Belczynski, K., Heger, A., Gladysz, W., et al. 2016, *A&A*, 594, A97, doi: [10.1051/0004-6361/201628980](https://doi.org/10.1051/0004-6361/201628980)

Belczynski, K., Hirschi, R., Kaiser, E. A., et al. 2020, *ApJ*, 890, 113, doi: [10.3847/1538-4357/ab6d77](https://doi.org/10.3847/1538-4357/ab6d77)

Binney, J., & Tremaine, S. 2008, *Galactic Dynamics*: Second Edition

Bondi, H. 1952, *MNRAS*, 112, 195, doi: [10.1093/mnras/112.2.195](https://doi.org/10.1093/mnras/112.2.195)

Bondi, H., & Hoyle, F. 1944, *MNRAS*, 104, 273, doi: [10.1093/mnras/104.5.273](https://doi.org/10.1093/mnras/104.5.273)

Borchers, A., Ye, C. S., & Fishbach, M. 2025, Gravitational-wave kicks impact spins of black holes from hierarchical mergers. <https://arxiv.org/abs/2503.21278>

Campanelli, M., Lousto, C., Zlochower, Y., & Merritt, D. 2007, *ApJL*, 659, L5, doi: [10.1086/516712](https://doi.org/10.1086/516712)

Centrella, J., Baker, J. G., Kelly, B. J., & van Meter, J. R. 2010, *Reviews of Modern Physics*, 82, 3069, doi: [10.1103/RevModPhys.82.3069](https://doi.org/10.1103/RevModPhys.82.3069)

Christensen-Dalsgaard, J., Dappen, W., Ajukov, S. V., et al. 1996, *Science*, 272, 1286, doi: [10.1126/science.272.5266.1286](https://doi.org/10.1126/science.272.5266.1286)

Davies, M. B., Church, R. P., Malmberg, D., et al. 2011, in *Astronomical Society of the Pacific Conference Series*, Vol. 439, *The Galactic Center: a Window to the Nuclear Environment of Disk Galaxies*, ed. M. R. Morris, Q. D. Wang, & F. Yuan, 212. <https://arxiv.org/abs/1002.0338>

Edgar, R. 2004, *NewAR*, 48, 843, doi: [10.1016/j.newar.2004.06.001](https://doi.org/10.1016/j.newar.2004.06.001)

Fishbach, M., Farr, W. M., & Holz, D. E. 2020, *ApJL*, 891, L31, doi: [10.3847/2041-8213/ab77c9](https://doi.org/10.3847/2041-8213/ab77c9)

Fishbach, M., Holz, D. E., & Farr, B. 2017, *ApJL*, 840, L24, doi: [10.3847/2041-8213/aa7045](https://doi.org/10.3847/2041-8213/aa7045)

Fragione, G., Grishin, E., Leigh, N. W. C., Perets, H. B., & Perna, R. 2018, *arXiv e-prints*, arXiv:1811.10627. <https://arxiv.org/abs/1811.10627>

Fragione, G., Kocsis, B., Rasio, F. A., & Silk, J. 2021, *arXiv e-prints*, arXiv:2107.04639. <https://arxiv.org/abs/2107.04639>

Fragione, G., Loeb, A., Kremer, K., & Rasio, F. A. 2020, *ApJ*, 897, 46, doi: [10.3847/1538-4357/ab94b2](https://doi.org/10.3847/1538-4357/ab94b2)

Fregeau, J. M., Joshi, K. J., Portegies Zwart, S. F., & Rasio, F. A. 2002, *ApJ*, 570, 171, doi: [10.1086/339576](https://doi.org/10.1086/339576)

Gammie, C. F., Shapiro, S. L., & McKinney, J. C. 2004, *ApJ*, 602, 312, doi: [10.1086/380996](https://doi.org/10.1086/380996)

Genzel, R., Eisenhauer, F., & Gillessen, S. 2010, *Rev. Mod. Phys.*, 82, 3121, doi: [10.1103/RevModPhys.82.3121](https://doi.org/10.1103/RevModPhys.82.3121)

Gerosa, D., & Fishbach, M. 2021, *Nature Astronomy*, 5, 749, doi: [10.1038/s41550-021-01398-w](https://doi.org/10.1038/s41550-021-01398-w)

Gerosa, D., & Moore, C. J. 2016, *Phys. Rev. Lett.*, 117, 011101, doi: [10.1103/PhysRevLett.117.011101](https://doi.org/10.1103/PhysRevLett.117.011101)

Gondán, L., Kocsis, B., Raffai, P., & Frei, Z. 2018, *ApJ*, 860, 5, doi: [10.3847/1538-4357/aabfee](https://doi.org/10.3847/1538-4357/aabfee)

González, J. A., Sperhake, U., Brügmann, B., Hannam, M., & Husa, S. 2007, *Phys. Rev. Lett.*, 98, 091101, doi: [10.1103/PhysRevLett.98.091101](https://doi.org/10.1103/PhysRevLett.98.091101)

González Prieto, E., Rodriguez, C. L., & Cabrera, T. 2025, *ApJL*, 990, L69, doi: [10.3847/2041-8213/adfd4a](https://doi.org/10.3847/2041-8213/adfd4a)

Grishin, E., Romero-Shaw, I. M., & Trani, A. A. 2025, *arXiv e-prints*, arXiv:2510.13066, doi: [10.48550/arXiv.2510.13066](https://doi.org/10.48550/arXiv.2510.13066)

Habibi, M., Gillessen, S., Pfuhl, O., et al. 2019, *ApJL*, 872, L15, doi: [10.3847/2041-8213/ab03cf](https://doi.org/10.3847/2041-8213/ab03cf)

Heger, A., Fryer, C. L., Woosley, S. E., Langer, N., & Hartmann, D. H. 2003, *The Astrophysical Journal*, 591, 288, doi: [10.1086/375341](https://doi.org/10.1086/375341)

Heggie, D. C. 1975, *MNRAS*, 173, 729, doi: [10.1093/mnras/173.3.729](https://doi.org/10.1093/mnras/173.3.729)

Hoang, B.-M., Naoz, S., Kocsis, B., Rasio, F. A., & Dosopoulou, F. 2018, *ApJ*, 856, 140, doi: [10.3847/1538-4357/aaafce](https://doi.org/10.3847/1538-4357/aaafce)

Hoang, B.-M., Naoz, S., & Kremer, K. 2020, *ApJ*, 903, 8, doi: [10.3847/1538-4357/abb66a](https://doi.org/10.3847/1538-4357/abb66a)

Hoang, B.-M., Naoz, S., & Sloneker, M. 2022, *ApJ*, 934, 54, doi: [10.3847/1538-4357/ac7787](https://doi.org/10.3847/1538-4357/ac7787)

Holley-Bockelmann, K., Gultekin, K., Shoemaker, D., & Yunes, N. 2008, *ApJ*, 686, 829, doi: [10.1086/591218](https://doi.org/10.1086/591218)

Hopman, C., & Alexander, T. 2005, *ApJ*, 629, 362, doi: [10.1086/431475](https://doi.org/10.1086/431475)

Hughes, S. A., & Blandford, R. D. 2003, *ApJL*, 585, L101, doi: [10.1086/375495](https://doi.org/10.1086/375495)

Jurado, C., Naoz, S., Lam, C. Y., & Hoang, B.-M. 2024, *ApJ*, 971, 95, doi: [10.3847/1538-4357/ad55ee](https://doi.org/10.3847/1538-4357/ad55ee)

Kim, T., & Goodman, J. 2026, On the Missing Red Giants near the Galactic Center. <https://arxiv.org/abs/2601.16191>

Kimball, C., Talbot, C., Berry, C. P. L., et al. 2021, *ApJL*, 915, L35, doi: [10.3847/2041-8213/ac0aef](https://doi.org/10.3847/2041-8213/ac0aef)

Kiroglu, F., Kremer, K., Biscoveanu, S., González Prieto, E., & Rasio, F. A. 2025a, *ApJ*, 979, 237, doi: [10.3847/1538-4357/ada26b](https://doi.org/10.3847/1538-4357/ada26b)

Kiroglu, F., Kremer, K., & Rasio, F. A. 2025b, *ApJL*, 994, L37, doi: [10.3847/2041-8213/ae1eeb](https://doi.org/10.3847/2041-8213/ae1eeb)

Kiroglu, F., Lombardi, J. C., Kremer, K., Vanderzanden, H. D., & Rasio, F. A. 2025c, *ApJL*, 983, L9, doi: [10.3847/2041-8213/adc263](https://doi.org/10.3847/2041-8213/adc263)

Kozai, Y. 1962, *AJ*, 67, 591, doi: [10.1086/108790](https://doi.org/10.1086/108790)

Kremer, K., Spera, M., Becker, D., et al. 2020, *ApJ*, 903, 45, doi: [10.3847/1538-4357/abb945](https://doi.org/10.3847/1538-4357/abb945)

Li, Z., & Bambi, C. 2014, *Journal of Cosmology and Astroparticle Physics*, 2014, 041–041, doi: [10.1088/1475-7516/2014/01/041](https://doi.org/10.1088/1475-7516/2014/01/041)

Lidov, M. L. 1962, *planss*, 9, 719, doi: [10.1016/0032-0633\(62\)90129-0](https://doi.org/10.1016/0032-0633(62)90129-0)

Limongi, M., & Chieffi, A. 2018, *ApJS*, 237, 13, doi: [10.3847/1538-4365/aacb24](https://doi.org/10.3847/1538-4365/aacb24)

Linial, I., & Sari, R. 2022, *ApJ*, 940, 101, doi: [10.3847/1538-4357/ac9bfd](https://doi.org/10.3847/1538-4357/ac9bfd)

Liu, B., & Lai, D. 2025, Hierarchical Black Hole Mergers in Nuclear Star Clusters: A Combined Dynamical-Secular Channel for GW231123-like Events. <https://arxiv.org/abs/2511.13820>

Löckmann, U., & Baumgardt, H. 2008, *MNRAS*, 384, 323, doi: [10.1111/j.1365-2966.2007.12699.x](https://doi.org/10.1111/j.1365-2966.2007.12699.x)

Lopez, Jr., M., Batta, A., Ramirez-Ruiz, E., Martinez, I., & Samsing, J. 2019, *ApJ*, 877, 56, doi: [10.3847/1538-4357/ab1842](https://doi.org/10.3847/1538-4357/ab1842)

Lousto, C. O., & Zlochower, Y. 2008, *PhRvD*, 77, 044028, doi: [10.1103/PhysRevD.77.044028](https://doi.org/10.1103/PhysRevD.77.044028)

Lousto, C. O., Zlochower, Y., Dotti, M., & Volonteri, M. 2012, *Phys. Rev. D*, 85, 084015, doi: [10.1103/PhysRevD.85.084015](https://doi.org/10.1103/PhysRevD.85.084015)

Magorrian, J., & Tremaine, S. 1999, *MNRAS*, 309, 447, doi: [10.1046/j.1365-8711.1999.02853.x](https://doi.org/10.1046/j.1365-8711.1999.02853.x)

Mai, A., Kremer, K., & Kiroglu, F. 2025, arXiv e-prints, arXiv:2510.21916, doi: [10.48550/arXiv.2510.21916](https://doi.org/10.48550/arXiv.2510.21916)

Mastrobuono-Battisti, A., Church, R. P., & Davies, M. B. 2021, *MNRAS*, 505, 3314, doi: [10.1093/mnras/stab1409](https://doi.org/10.1093/mnras/stab1409)

Merritt, D. 2006, *Reports on Progress in Physics*, 69, 2513, doi: [10.1088/0034-4885/69/9/R01](https://doi.org/10.1088/0034-4885/69/9/R01)

Miller, M. C., & Lauburg, V. M. 2009, *ApJ*, 692, 917, doi: [10.1088/0004-637X/692/1/917](https://doi.org/10.1088/0004-637X/692/1/917)

Naoz, S. 2016, *ARA&A*, 54, 441, doi: [10.1146/annurev-astro-081915-023315](https://doi.org/10.1146/annurev-astro-081915-023315)

Naoz, S., Farr, W. M., Lithwick, Y., Rasio, F. A., & Teyssandier, J. 2013a, *MNRAS*, 431, 2155, doi: [10.1093/mnras/stt302](https://doi.org/10.1093/mnras/stt302)

Naoz, S., Kocsis, B., Loeb, A., & Yunes, N. 2013b, *ApJ*, 773, 187, doi: [10.1088/0004-637X/773/2/187](https://doi.org/10.1088/0004-637X/773/2/187)

Naoz, S., Rose, S. C., Michaely, E., et al. 2022, *ApJL*, 927, L18, doi: [10.3847/2041-8213/ac574b](https://doi.org/10.3847/2041-8213/ac574b)

O’Leary, R. M., Kocsis, B., & Loeb, A. 2009, *MNRAS*, 395, 2127, doi: [10.1111/j.1365-2966.2009.14653.x](https://doi.org/10.1111/j.1365-2966.2009.14653.x)

O’Leary, R. M., Rasio, F. A., Fregeau, J. M., Ivanova, N., & O’Shaughnessy, R. 2006, *ApJ*, 637, 937, doi: [10.1086/498446](https://doi.org/10.1086/498446)

Peters, P. C. 1964, *Physical Review*, 136, 1224, doi: [10.1103/PhysRev.136.B1224](https://doi.org/10.1103/PhysRev.136.B1224)

Peters, P. C., & Mathews, J. 1963, *Physical Review*, 131, 435, doi: [10.1103/PhysRev.131.435](https://doi.org/10.1103/PhysRev.131.435)

Preto, M., & Amaro-Seoane, P. 2010, *ApJL*, 708, L42, doi: [10.1088/2041-8205/708/1/L42](https://doi.org/10.1088/2041-8205/708/1/L42)

Quinlan, G. D., & Shapiro, S. L. 1987, *ApJ*, 321, 199, doi: [10.1086/165624](https://doi.org/10.1086/165624)

Radia, M., Sperhake, U., Berti, E., & Croft, R. 2021, *PhRvD*, 103, 104006, doi: [10.1103/PhysRevD.103.104006](https://doi.org/10.1103/PhysRevD.103.104006)

Reisswig, C., Husa, S., Rezzolla, L., et al. 2009, *PhRvD*, 80, 124026, doi: [10.1103/PhysRevD.80.124026](https://doi.org/10.1103/PhysRevD.80.124026)

Renzo, M., Farmer, R., Justham, S., et al. 2020, *A&A*, 640, A56, doi: [10.1051/0004-6361/202037710](https://doi.org/10.1051/0004-6361/202037710)

Rizzuto, F. P., Naab, T., Spurzem, R., et al. 2022, *MNRAS*, doi: [10.1093/mnras/stac231](https://doi.org/10.1093/mnras/stac231)

Rodriguez, C. L., Amaro-Seoane, P., Chatterjee, S., & Rasio, F. A. 2018, *PhRvL*, 120, 151101, doi: [10.1103/PhysRevLett.120.151101](https://doi.org/10.1103/PhysRevLett.120.151101)

Rodriguez, C. L., Zevin, M., Amaro-Seoane, P., et al. 2019, *Phys. Rev. D*, 100, 043027, doi: [10.1103/PhysRevD.100.043027](https://doi.org/10.1103/PhysRevD.100.043027)

Rodriguez, C. L., Weatherford, N. C., Coughlin, S. C., et al. 2022, *ApJS*, 258, 22, doi: [10.3847/1538-4365/ac2edf](https://doi.org/10.3847/1538-4365/ac2edf)

Rom, B., Linial, I., Kaur, K., & Sari, R. 2024a, *ApJ*, 977, 7, doi: [10.3847/1538-4357/ad8b1d](https://doi.org/10.3847/1538-4357/ad8b1d)

Rom, B., Sari, R., & Lai, D. 2024b, *ApJ*, 964, 43, doi: [10.3847/1538-4357/ad284b](https://doi.org/10.3847/1538-4357/ad284b)

Rose, S. C., & Mockler, B. 2025, *ApJL*, 985, L40, doi: [10.3847/2041-8213/add266](https://doi.org/10.3847/2041-8213/add266)

Rose, S. C., Naoz, S., Gautam, A. K., et al. 2020, *ApJ*, 904, 113, doi: [10.3847/1538-4357/abc557](https://doi.org/10.3847/1538-4357/abc557)

Rose, S. C., Naoz, S., Sari, R., & Linial, I. 2022, *ApJL*, 929, L22, doi: [10.3847/2041-8213/ac6426](https://doi.org/10.3847/2041-8213/ac6426)

—. 2023, arXiv e-prints, arXiv:2304.10569, doi: [10.48550/arXiv.2304.10569](https://doi.org/10.48550/arXiv.2304.10569)

Sakstein, J., Croon, D., McDermott, S. D., Straight, M. C., & Baxter, E. J. 2020, arXiv e-prints, arXiv:2009.01213. <https://arxiv.org/abs/2009.01213>

Sari, R., & Fragione, G. 2019, *ApJ*, 885, 24, doi: [10.3847/1538-4357/ab43df](https://doi.org/10.3847/1538-4357/ab43df)

Schnittman, J. D., & Buonanno, A. 2007, *ApJL*, 662, L63, doi: [10.1086/519309](https://doi.org/10.1086/519309)

Schödel, R., Nogueras-Lara, F., Gallego-Cano, E., et al. 2020, *A&A*, 641, A102, doi: [10.1051/0004-6361/201936688](https://doi.org/10.1051/0004-6361/201936688)

Shima, E., Matsuda, T., Takeda, H., & Sawada, K. 1985, *MNRAS*, 217, 367, doi: [10.1093/mnras/217.2.367](https://doi.org/10.1093/mnras/217.2.367)

Sidhu, J. S., Rose, S. C., & Rasio, F. A. 2025, arXiv e-prints. <https://arxiv.org/abs/2512.11175>

Sopuerta, C. F., Yunes, N., & Laguna, P. 2007, *ApJL*, 656, L9, doi: [10.1086/512067](https://doi.org/10.1086/512067)

Spera, M., & Mapelli, M. 2017, *MNRAS*, 470, 4739, doi: [10.1093/mnras/stx1576](https://doi.org/10.1093/mnras/stx1576)

Sperhake, U., Rosca-Mead, R., Gerosa, D., & Berti, E. 2020, *PhRvD*, 101, 024044, doi: [10.1103/PhysRevD.101.024044](https://doi.org/10.1103/PhysRevD.101.024044)

Spitzer, L. 1987, *Dynamical evolution of globular clusters*

Stegmann, J., Antonini, F., Olejak, A., et al. 2025, arXiv e-prints, arXiv:2512.15873. <https://arxiv.org/abs/2512.15873>

Stephan, A. P., Naoz, S., Ghez, A. M., et al. 2016, *MNRAS*, 460, 3494, doi: [10.1093/mnras/stw1220](https://doi.org/10.1093/mnras/stw1220)

Stone, N. C., & Metzger, B. D. 2016, *MNRAS*, 455, 859, doi: [10.1093/mnras/stv2281](https://doi.org/10.1093/mnras/stv2281)

Su, Y. 2025, arXiv e-prints, arXiv:2501.16258, doi: [10.48550/arXiv.2501.16258](https://doi.org/10.48550/arXiv.2501.16258)

Tagawa, H., Haiman, Z., Bartos, I., Kocsis, B., & Omukai, K. 2021, *Monthly Notices of the Royal Astronomical Society*, 507, 3362, doi: [10.1093/mnras/stab2315](https://doi.org/10.1093/mnras/stab2315)

Tong, H., Callister, T. A., Fishbach, M., et al. 2025, arXiv e-prints, arXiv:2511.05316. <https://arxiv.org/abs/2511.05316>

Vink, J. S., Higgins, E. R., Sander, A. A. C., & Sabhahit, G. N. 2021, *MNRAS*, 504, 146, doi: [10.1093/mnras/stab842](https://doi.org/10.1093/mnras/stab842)

Volonteri, M., Madau, P., Quataert, E., & Rees, M. J. 2005, *ApJ*, 620, 69, doi: [10.1086/426858](https://doi.org/10.1086/426858)

Volonteri, M., Sikora, M., Lasota, J.-P., & Merloni, A. 2013, *The Astrophysical Journal*, 775, 94, doi: [10.1088/0004-637X/775/2/94](https://doi.org/10.1088/0004-637X/775/2/94)

Wang, J., & Merritt, D. 2004, *ApJ*, 600, 149, doi: [10.1086/379767](https://doi.org/10.1086/379767)

Woosley, S. E. 2017, *The Astrophysical Journal*, 836, 244, doi: [10.3847/1538-4357/836/2/244](https://doi.org/10.3847/1538-4357/836/2/244)